Numerical reconstruction of porous architecture for suspension plasma sprayed coatings

Yongli Zhao, Zhimeng Yang, Juhong Wen, Marie-Pierre Planche, François Peyraut, Jan Ilavsky, Bertrand Lenoir, Hanlin Liao, Ghislain Montavon, Audrey Lasalle, et al.

Numerical reconstruction of porous architecture for suspension plasma sprayed coatings

Yongli Zhao, Juhong Wen, Zhimeng Yang
School of Mechanical and Automotive Engineering, Shanghai University of Engineering Science, 201620, China Place
zyl@sues.edu.cn

Marie-Pierre Planche, François Peyraut, Hanlin Liao, Ghislain Montavon
ICB UMR 6303, CNRS, Université de Bourgogne Franche-Comté, UTBM, 90010 Belfort, France
marie-pierre.planche@utbm.fr

Jan Ilavsky
Advanced Photon Source, Argonne National Laboratory, 9700 S. Cass Avenue, Argonne, IL 60439, USA
ilavsky@anl.gov

Bertrand Lenoir
Institut Jean Lamour, UMR 7198 CNRS, Université de Lorraine, 54011 Nancy, France
bertrand.lenoir@univ-lorraine.fr

Abstract (Optional)

The porous architecture of coatings has a significant influence on the coating performances and thus should be properly designed for the intended applications. For simulating the coating properties, it is necessary to determine the numerical representation of the coating microstructure. In this study, YSZ coatings were manufactured by suspension plasma spray (SPS). Afterwards, the porous architecture of as-prepared coatings was investigated by the combination of three techniques, imaging analysis, Ultra Small Angle X-ray Scattering (USAXS), and X-ray transmission. A microstructural model for reconstructing the porous architecture of the SPS coating was subsequently computed according to the collected experimental results. Finally, the coating thermal properties were simulated based on the model and were compared with the experimental results.

Introduction

It has been proven that finely structured or nanostructured coatings exhibit superior performances compared to the micrometer-sized coatings [1-3], such as lower thermal conductivity [4], higher wear resistance [5], and improved friction coefficient [6]. Due to the superior ability to manufacture such fine structure coatings, suspension plasma spray (SPS) has continuously gained increasing interest in the last decade. As for the micrometer-sized coatings, the SPS coating properties have a close relationship with its microstructure. For example, the coating properties strongly depend on its porous architecture [4, 7]. Therefore, the coating porous architecture should be properly designed for the intended applications.

Numerical simulation is considered as a powerful tool to understand the relationship between the microstructure and coating properties. In order to efficiently perform the simulation, it is necessary to determine the adapted numerical model of the coating microstructure. Accurate simulation is dependent on the models which are able to closely mimic the microstructure of the actual coatings. Since the coating performances strongly depend on its porous architecture, in-depth understanding of the microscopic characteristics of the coating is necessary : such numerical models should include as much details as possible about the coating porous architecture focused on the pore sizes, the pore shapes, and their corresponding proportions. The accurate characterization of coating porous architecture is therefore the crucial first step for the numerical reconstruction of SPS coatings.

However, it is challenging to characterize thereforeevaluate the porous architecture of SPS coatings [8]. As such coatings are deposited by the piling up of particles with a size ranging from a few tens of nanometers to a few micrometers on the substrate, the coating formation is very complicated and the pores in SPS coatings are distributed over a wide size range, from nanometers to micrometers even to millimeters. Commonly, the measurement of pores can be performed with numerous techniques using imaging [9], physical [7, 10], and electrochemical [10] approaches. However, the limited SEM resolution makes the imaging approach difficult to take into consideration the small pores, especially the nano pores. The requirement of the liquid or gas phase penetrating inside the material causes the failure of physical and electrochemical approaches to detect the closed pores. Therefore, it is difficult to accurately characterize the porous architechture of SPS coatings by using these common methods.

To solve the challenges in characterization of the nano-submicro pores, Ultra-Small Angle X-ray Scattering (USAXS) can be applied due to its unprecedented capability in measuring very small pore sizes [11]. But USAXS is not suitable to measure pores over a few micrometer in size. In order to overcome the shortcoming of USAXS, imaging method can be used as a complementary technique for characterizing the micro-sized pores. Due to the quality of SEM images (i.e. the contrast of image) could affect the

accuracy of measurement result, the coating total porosity measured using X-ray transmission can be employed to correct the imaging analysis, as this technique is a non-destructive test without any limitation of resolution [12]. Through the combination of these three techniques, the accurate characterization of the coating porous architecture in the global size range could be done.

In the current study, Yttria-stabilized Zirconia (YSZ) coatings with different porosities were firstly manufactured by SPS technique. The porous architecture of the coatings was then investigated by the combination of three techniques, Ultra Small Angle X-ray Scattering (USAXS), imaging analysis, and X-ray transmission. Afterwards, by analyzing the experimental data obtained with the different techniques, the pore size distribution of the coating in the global size range was quantified. A numerical model for reconstructing the porous architecture of SPS coatings was subsequently computed according to the collected experimental results. Finally, the thermal properties of the coatings were simulated based on the numerical model and were compared with the experimental results.

Experimental procedure

Materials and coating manufacturing

The atmospheric plasma ProPlasma torch (Saint-Gobain Coating Solutions, Avignon, France) equipped with a 6.5 mm diameter anode and worked on the "high performance" mode was used to manufacture the SPS coatings. The working gases were a mixture of 50 L/min Argon and 10 L/min Hydrogen and the applied electric power was equal to 41 kW. YSZ powders (8 wt.% yttria, 3 wt.% alumina, Saint-Gobain ZirPro Co., Ltd.) with different particle sizes and different mass load were dispersed in ethanol to prepare suspensions. A twin-fluid atomizer was used to inject the suspension into the plasma jet and the suspension feed rate was equal to about 45 g/min in all experiments. Stainless steel (304L, thickness = 10 mm, diameter = 25 mm) was used as substrate. The details of the coating manufacturing can be viewed at our previous work [11]. The main process parameters of fabrication are listed in Table 1.

Table 1: Process parameters of the experimental runs to prepare coatings

Sample No.	Suspension mass load (wt.%)	Powder size (μm)	Spray distance (mm)	Spray step (mm)	Substrate roughness (μm)
S1	25	0.36	40	6	0.16
S2	20	0.1	40	6	2.45
S3	25	0.23	40	6	2.45
S4	20	0.36	40	3	3.51
S5	25	0.36	50	12	3.51

Characterization methods

The microstructural analyses of the as-sprayed SPS coatings were performed on the cross sections using the field emission scanning electron microscopy (JSM-7800F, JEOL, Japan). Specimens for cross-section analysis were sectioned using a diamond cutting blade and then mounted in resin. Samples were subsequently grinded with emery papers, polished with diamond paste, and cleaned with water and ethanol in an ultra-sonic bath. All observed samples were sputtered with a thin gold layer to allow the ceramic layers to be observed clearly.

Ultra-Small-Angle X-ray Scattering was employed to evaluate the nano/submicro pores in the YSZ coatings [11]. They were carried out at 9ID-C USAXS/SAXS/WAXS instrument (Argonne National Laboratory, Argonne, IL, USA) and the spanning extended range of scattering vectors, q, is from 10-4 to 1 Å-1 [10, 13] .Scattering data were reduced using data reduction programs Indra and Nika [14]. Data were placed on absolute intensity scale using standard instrument calibration methods. Size distribution of pores was analyzed using Irena package [15]. X-ray transmission technique was used to measure the total porosity of the as prepared SPS coatings. They were also carried out at the same instrument for USXAS. Prior to the measurements, the SPS coatings were removed from substrates by acid pickling in Aqua Regia (nitro-hydrochloric acid). The free-standing coatings were cleaned with deionized water and ethanol and then were dried in air environment.

The thermal diffusivity of as-sprayed SPS coatings were measured with the laser-flash technique on a LFA 427 (Netzsch, Germany) in the temperature 25 ℃. The thermal diffusivity, determined using the improved Cape-Lehmann model [19], was then used to calculate the thermal conductivity λ via the formula:

$$\lambda=\alpha\times C\_p\times\rho \qquad \text{Eq. 1}$$

where Cp is the specific heat capacity and ρ the density of coating. The specific heat capacity of the YSZ material was measured using a DSC 404C differential scanning calorimeter (Netzsch, Germany). The density of coating was calculated via the following expression:

$$\rho=\rho_0\times(1-P_t) \qquad \text{Eq. 2}$$

where ρ_0 is the density of dense YSZ powder (5 mol% Y_2O_3 stabilized zirconia powder) which was estimated on 6.0 g/cm^3 and P_t is the total porosity of SPS coating.

Porous architecture quantification and results

Coating microstructure

The microstructure of SPS coating is highly related to the thermal spray process, in which the suspension is firstly fragmented and evaporated, then the material powders are melted and finally impact on the substrate with a high speed. Due to the existence of the not-well-melted particles and the re-solidification of particles before impact, some pores could be formed in the gap in between these particles. The typical SEM images of as-prepared SPS coating are shown in Fig.1. It can be seen that the coating exhibits a porous structure and the

pores are in a wide size range from nanometer up to several micrometers, as the arrows indicate in Fig.1(b).

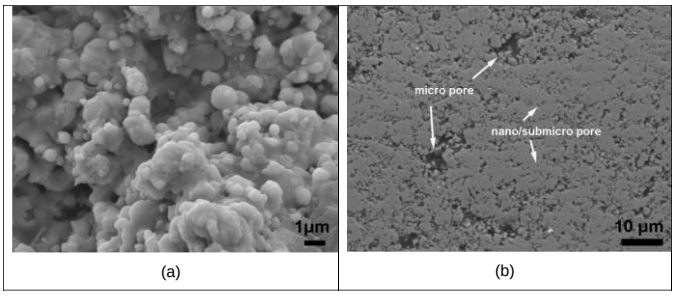

Figure 1: Typical SEM images of as prepared SPS coating: a) top surface, and b) cross-section

Quantitative analysis of nano/submicro pores

Ultra-small angle x-ray scattering (USAXS) is a well-established technique for studying nanoscale materials [16]. When a X-ray beam travels through a porous sample, some of the X-rays are scattered out of the incident beam direction by a small angle. The scattering pattern in USAXS is a function of a scattering vector q, which is related to the scattering angle and the x-ray wavelength by:

$$q=4\pi/(\lambda \sin(\theta)) \qquad \text{Eq.3}$$

where λ is the wavelength of the X rays and 2θ is the scattering angle. The trend in scattering intensity vs. scattering vector q, as depicted in Fig.2, can be used to quantitatively measure the size and shape of pores in a feature scale range from a few nanometers up to more than a micrometer. Combining the equation Eq.1 with Bragg's law, the pore diameter d, probed at a given q range follows the general inverse relationship:

$$d=2\pi/q \qquad \text{Eq.4}$$

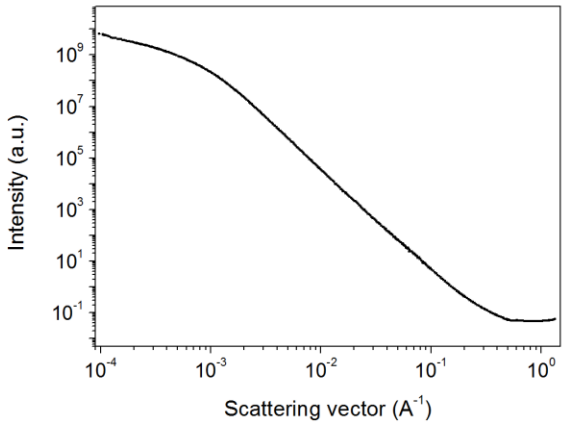

Figure 2: Scattered X-ray intensity as function of scattering vector for a typical SPS coating

The quantitative analysis of nano/submicro pores based on the USAXS results are presented in Fig.3. In the pore size range smaller than 1 micron, the pore number is roughly decreased as the pore diameter increases, from about 1015/ mm3 down to about 106/ mm3. The content of these nano/submicro pores in the coating is also calculated by integrating their size distributions over all sizes. It varied in a large range with about 10% for coating S1 and about 15% for coating S2. From the results of cumulative percentages displayed in Fig.3, one can observe that about 60% of the nano-submicro pores in all coatings are smaller than 100 nm. One other interesting insight is that 90% of the nano-submicro pores are smaller than 360 nm, which is the biggest size of initial powders used in this study.

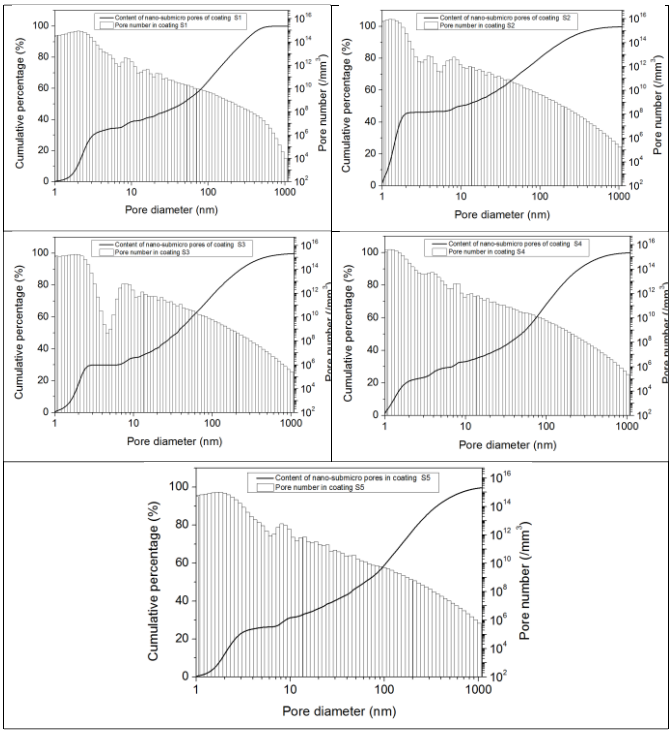

Figure 3: Nano/submicro pore size distribution analyzed based on USAXS results

Quantitative analysis of micro-sized pores

Imaging analysis based on the SEM cross section images was employed to evaluate the micro-sized pores of as prepared coatings. In a SEM image of the SPS coating, as shown in Fig.4a, the dark gray parts represent the pores and in contrast the gray elements correspond to YSZ material. In order to separate the pores (the dark gray parts) from the SEM image, a binary image (Fig.4b) was produced firstly by thresholding the original gray-scale image (Fig.4a). In the binary image of Fig.4b, the black phase is the pores, and white phase the YSZ material. One can see that although the binary image contains much less information than its gray-scale counterpart, it embodies the information of sizes, shapes and positions of the pores. Binary image has only two gray levels and is therefore represented using only one bit per pixel. Numerically, the two levels are set as 0 for the black phase and 255 for the white phase. Fig.4c displays part of the matrix data of the binary image of Fig.4.b, which consists of the pixels with value 0 (the pores) and the pixels with value 255 (YSZ material). According to the matrix data, it is easy to calculate the pore

area by summing the adjacent pixels with the value of 0. In this study, the pore shape is assumed to be circular, the diameter of the pore (d) can thereby be calculated by the following formula:

$$d=2\sqrt{(S/\pi)} \qquad \text{Eq.5}$$

where s is the pore area. Finally, according to the statistical results, the pore size distribution can be obtained as shown in Fig.4d. It should be noted that the unit of pore diameter is pixel in Fig.4d. The actual physical distance can be calibrated using the scale bar of the original SEM image.

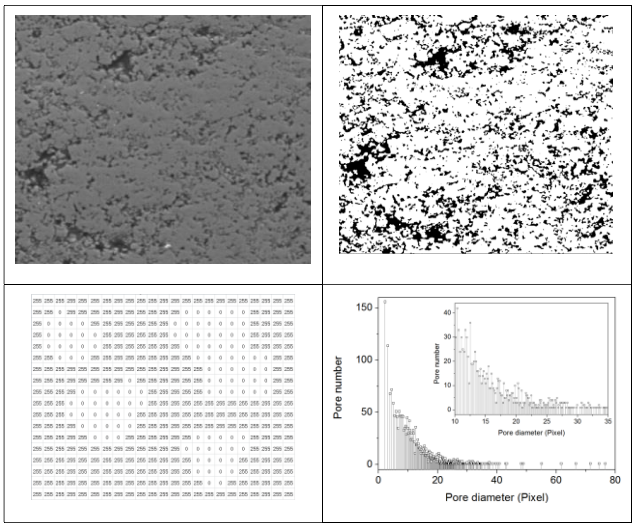

Figure 4: Process of imaging method to analyze the porous architecture: a) Original SEM image of coating, b) Binary image converted from the SEM image, c) Matrix data extracted from the binary image, and d) Statistical result of the pore size distribution

In this work, for collecting enough statistic information on the micro-sized pores of the SPS coating, ten SEM images were collected randomly on each sample across its entire cross-section in regions not close to the edges. In order to minimize the measurement error, all the samples were prepared under the same conditions, and all the SEM images were taken under identical conditions (1000X, 15 kV, WD = 10 mm). These SEM images were converted into binary images and then analyzed according to the method described above, and the results are shown in Fig.5. It can be seen that:

- The micro-sized pores in the as prepared SPS coatings are mainly distributed in the range of tens of microns. Furthermore, more than 50% of the micro-sized pores are smaller than 5 μm.
- As the trend observed for nano/submicro pores, the number of micro pores in the coatings is also reduced with the increase of the pore size, from about 10^6 / mm^3 down to about several thousand per mm^3.
- With regard to the smaller pores, especially smaller than 5 μm, the pore diameters are approximately continuous. In contrast, while the pores rise to larger sizes, the pore diameters become more discrete.

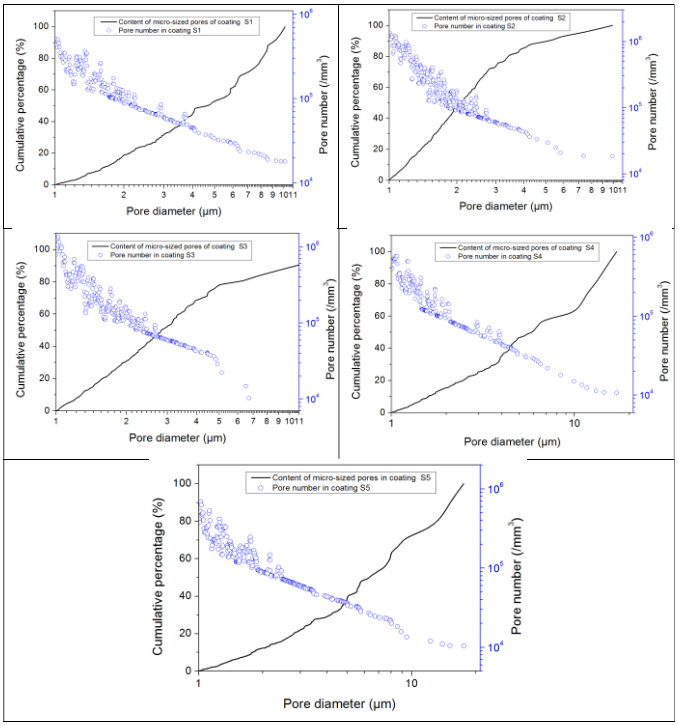

Figure 5: Pore size distribution in micron scale analyzed according to imaging method

Numerical reconstruction of porous architecture

Based on the collected data of the previous section, we used a stochastic method to reconstruct the porous architecture of SPS coatings. To simplify the modeling, the coating was assumed as a two-dimensional (2D) panel containing N × N lattices, although it can be extended to a three-dimensional (3D) system. The area of each lattice is denoted by s, which is also equal to the area of the smallest pore in the coating. That is to say, if the minimum pore area simulated is 1 nm2, to model a 2D panel with 1 × 1 mm2, the number of 1012 lattices is required. In this work, the pore is hypothesized as a group of compact adjacent lattices randomly distributed in the two-dimensional panel.

Figure 6 presents a summary of the flowchart describing the modeling algorithm. Firstly, the pores with different sizes are generated according to the data collected in section 3. The largest pores were then randomly assigned in the two-dimensional panel. An iterative arrangement algorithm is developed to avoid the overlapping (one pore may be assigned on the location which has been occupied by other pores). During each iteration, the smaller pore is selected for reassignment until the overlap is eliminated. This procedure is executed cyclically until all pores are registered in the 2D panel. Figure 7 provides an illustration describing the reconstruction process of a porous coating with three different pore sizes.

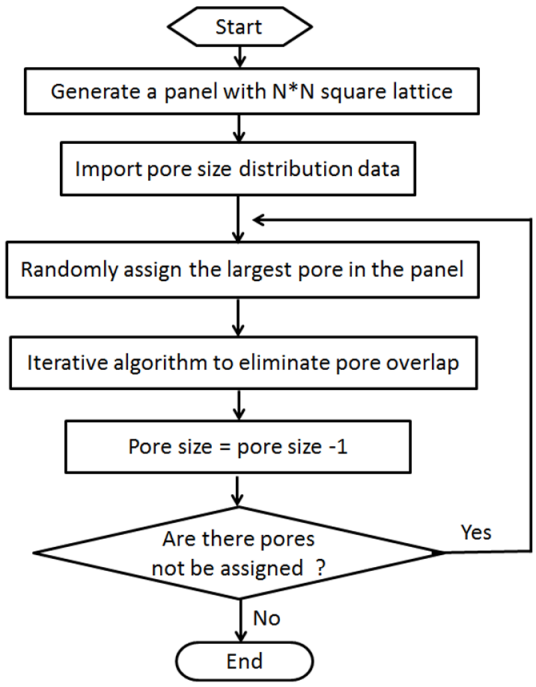

Figure 6: Program flowchart of numerical reconstruction of coating porous architecture

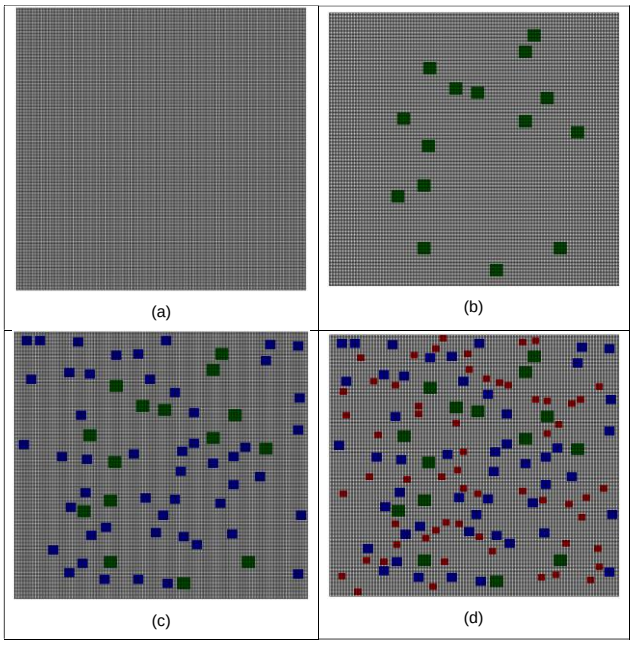

Figure 7: Schematic of the numerical reconstruction process: a) Initialization of a dense coating, b) Largest pores are randomly assigned, c) Medium-sized pores are randomly assigned, and c) Smallest pores are randomly assigned

Discussion

Comparison of USAXS and imaging method at submicron scale

Commonly, image analysis using SEM images taken at sufficiently high magnification could be used to estimate the porosity of coatings [7, 17, 18]. However, even if imaging is relatively easy to carry out and inexpensive, it has the limitation to detect the small pores, in particular for pores at the nanometer scale, due to the limited resolution of the SEM images. That may lead to an underestimation of the real porosity. In order to study the characterization accuracy of the imaging method, it was compared with the results of USAXS, as presented in Fig.8. It can be seen that:

- At the submicron scale, the pore number measured using imaging method is less than that detected by USAXS. Forthermore, the smaller the pore diameter, the larger the difference between the two characterization techniques. This difference should be caused by the limitation of the SEM image resolution, as some small pores could not be clearly distinguished from the SEM image.
- While the pore sizes are larger than 500 nm, the results obtained from the two techniques are almost the same, which means that imaging method is sufficient to accurately detect the small pores over this size range. On the other hand, it indicates that the current study is rigorous as imaging method was not employed to characterize the nano/submicron pores.
- It should be noted that, in the size range from about 500 nm to 1μm, the pore number measured by image method is slightly more than that obtained by USAXS. This can be attributed to the coating damage during the sample preparation for SEM observation, for example some splats could be pull out during the polishing process.

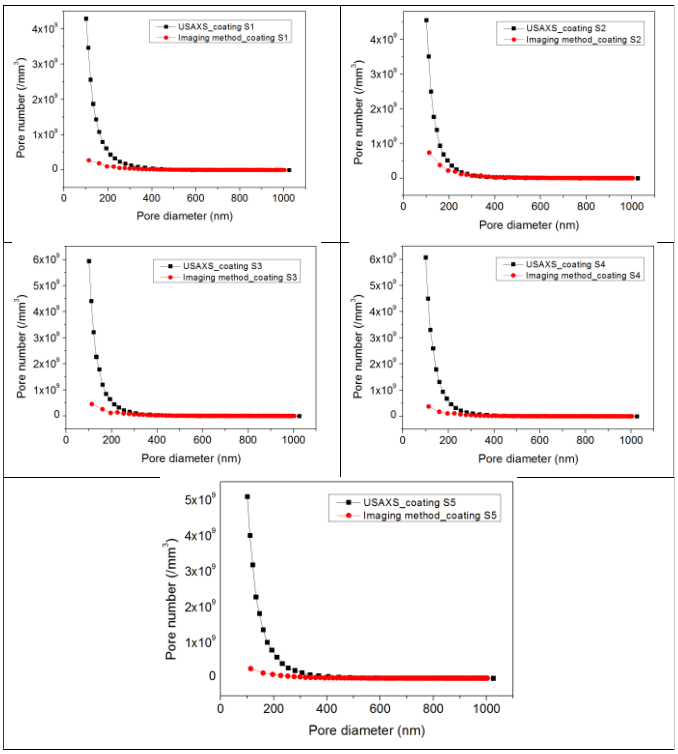

Figure 8: Comparison of pore characterization with USAXS and imaging method at submicron scale

Verification of the quantification results

As discussed above, the quantification of the coating porous architecture in the current work is divided into two separate

parts, the quantitative analysis of the nano/submicro pores and the micro-sized pores. In order to verify the experimental results, the total porosities of all as prepared coatings were measured using x-ray transmission. Although this technique cannot provide the information on the size and the shape of pores, it can accurately measure the total porosity because it has the advantage of allowing a resolution without limitation [12]. Since the nano/submicro pores and the micro-sized pores have been characterized by USAXS and imaging method respectively, assuming the two methods are accurate enough, the coating total porosity should be the sum of their contents:

$$P_{tc}=P_n+P_m \qquad \text{Eq.6}$$

where P_{tc} represents the calculated total porosity, P_n the content of the pores smaller than 1 μm, and P_m the content of the pores larger than 1 μm.

Figure 9 presents the comparison of the coatings' total porosities measured using x-ray transmission and calculated according to Eq.4. A good agreement could be found between the two results. This validates, otherwise the effectiveness of the combination techniques (USAXS and imaging method) to quantify the total porous architecture for SPS coatings. Nevertheless, one can see that the calculated total porosities are slightly higher than the experimental values. This may be caused by the coating damage during the sample preparation for the SEM observation.

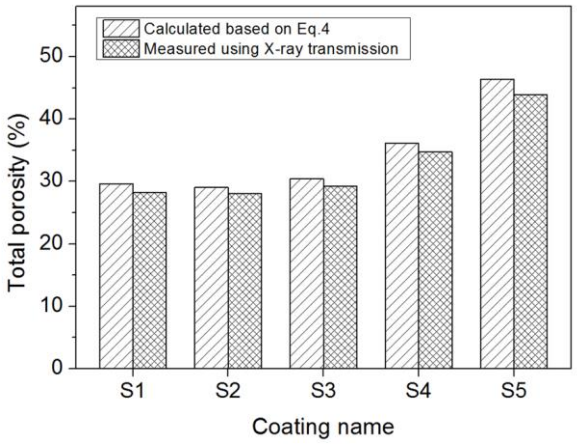

Figure 9: Coating total porosities measured using X-Ray transmission and calculated according to Eq.6

Application of the numerical porous architecture model

Due to its low thermal conductivity and high thermal expansion coefficient, Yttria-stabilized Zirconia (YSZ) was widely used as a thermal barrier coatings (TBCs) top coat material [19]. Its thermal resistance strongly depends on the coating microstructure. Therefore, the porous architecture of the YSZ layer needs to be carefully considered for improving the performance of TBCs. Although experiments can fully reveal the relationship between coating microstructure and its performance, simulation method could be considered as a time-saving and more economical method.

In this work, the thermal conductivities of the SPS coatings were simulated based on the numerical model developed in section 4. It was performed by considering the coating as a two-phase medium, the solid phase (YSZ material) and the gas phase (air entrapped in the pores). The thermal conductivity of the solid phase was set to be 2.5 $Wm^{-1}K^{-1}$ [20], and the gas phase was assigned via the formula [10, 20, 21]:

$$\lambda_{gas}=\lambda_{atm}\ 1/(1+CT/(Pd)) \qquad \text{Eq.7}$$

where λ_{gas} is the gas conductivity at room temperature and atmospheric pressure (0.025 $Wm^{-1}K^{-1}$), d is the pore size. The simulation results of coatings' thermal conductivities are shown in Fig.10. It is found that they are in good agreement with the experimental results. Hence, the numerical porous architecture model proposed in this work could provide a valuable guidance for the designing of thermal barrier coatings.

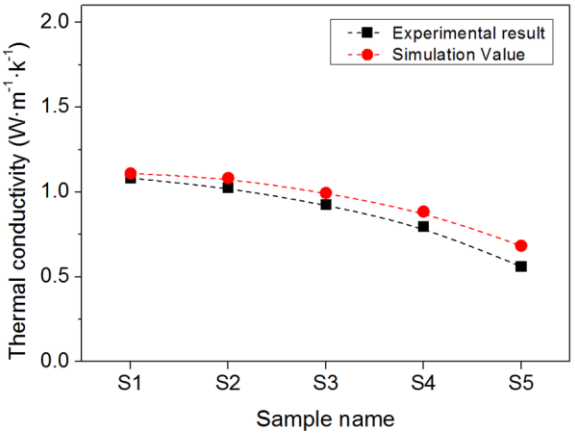

Figure10: Thermal conductivities of the experimental results and simulated values

Conclusions

Suspension plasma sprayed YSZ coatings with different porous architecture were fabricated. Their porous architectures were accurately quantified by the combination of USAXS and image analysis techniques. The quantitative efficiency was verified using x-ray transmission technique. The results showed that imaging method is suitable for characterizing pores at the micro-sized scale, and USAXS has satisfying capability in measuring nano pores. Moreover, a numerical porous architecture model of the SPS coating was developed according to the collected experimental results. The thermal properties of the coatings were simulated based on the model. The simulated results showed good agreement with the experimental data, which indicates the high effectiveness of the numerical reconstruction method for SPS coatings. In addition to the predicting the thermal properties fit pretty well with the experimental results, leading to consider that this approach could be used to design SPS coatings for extending their applications.

Acknowledgments

This research used resources of the Advanced Photon Source, a U.S. Department of Energy (DOE) Office of Science User Facility operated for the DOE Office of Science by Argonne National Laboratory under Contract No. DE-AC02-06CH11357. This research was also sponsored by startup research foundation of Shanghai University of Engineering Science No. 201980. The authors are grateful to the financial supports by Bourgogne Franche Comte Region [Grant N° 2019-7-09410].

References

[1] A. Vardelle, M. Christian, and A. Jun, The 2016 Thermal Spray Roadmap. Journal of Thermal Spray Technology, 2016. 25(3): p. 1376-1440.
[2] P. Fauchais, G. Montavon, and B.R. Marple, Engineering a new class of thermal spray nano-based microstructures from agglomerated nanostructured particles, suspensions and solutions. an invited review. Journal of Physics D: Applied Physics, 2011. 44: p. 93001-1-93001-53.
[3] A. Joulia et al., Tailoring the Spray Conditions for Suspension Plasma Spraying. Journal of Thermal Spray Technology, 2015. 24(1): p. 24-29
[4] Y. Zhao et al., Porous architecture and thermal properties of thermal barrier coatings deposited by suspension plasma spray. Surface and Coatings Technology, 2020. 386: p. 125462.
[5] Y. Wang et al., A novel structured suspension plasma sprayed YSZ-PTFE composite coating with tribological performance improvement. Surface and Coatings Technology, 2019. 358: p. 108-113.
[6] Y. Zhao et al., Microstructural, mechanical and tribological properties of suspension plasma sprayed YSZ/h-BN composite coating. Journal of the European Ceramic Society, 2018. 38(13): p. 4512-4522.
[7] U. Klement, J. Ekberg, and S.T. Kelly, 3D Analysis of Porosity in a Ceramic Coating Using X-ray Microscopy. Journal of Thermal Spray Technology, 2017. 26(3): p. 456-463.
[8] J.Ekberg et al., The Influence of Heat Treatments on the Porosity of Suspension Plasma-Sprayed Yttria-Stabilized Zirconia Coatings. Journal of Thermal Spray Technology, 2018.
[9] Y. Zhao et al., Experiments, Statistical Analysis, and Modeling to Evaluate the Porosity Influence in SPS Coatings. Journal of Thermal Spray Technology, 2019. 28: p. 76-86.
[10] A.Bacciochini et al., Quantification of void network architectures of suspension plasma-sprayed (SPS) yttria-stabilized zirconia (YSZ) coatings using Ultra-small-angle X-ray scattering (USAXS). Materials Science and Engineering: A, 2010. 528(1): p. 91-102.
[11] Y.Zhao et al., Evaluation of nano/submicro pores in suspension plasma sprayed YSZ coatings. Surface and Coatings Technology, 2019: p. 125001.
[12] Y.Zhao et al., Parametric Analysis and Modeling for the Porosity Prediction in Suspension Plasma-Sprayed Coatings. Journal of Thermal Spray Technology, 2020. 29(1): p. 51-59.
[13] K. Kishitake, H. Era, and F. Otsubo, Characterization of plasma sprayed Fe-17Cr-38Mo-4C amorphous coatings crystallizing at extremely high temperature. Journal of Thermal Spray Technology, 1996. 5(3): p. 283-288.
[14] J. Ilavsky et al., Development of combined microstructure and structure characterization facility for in situ and operando studies at the Advanced Photon Source. Journal of Applied Crystallography, 2018. 51(3): p. 867-882.
[15] J. Ilavsky and P.R. Jemian, Irena: tool suite for modeling and analysis of small-angle scattering. Journal of Applied Crystallography, 2009. 42(2): p. 347-353.
[16] J. Ilavsky et al., Ultra-Small-Angle X-ray Scattering Instrument at the Advanced Photon Source: History, Recent Development, and Current Status. Metallurgical and Materials Transactions A, 2013. 44(1): p. 68-76.
[17] P. Sokołowski et al., The microstructural studies of suspension plasma sprayed zirconia coatings with the use of high-energy plasma torches. Surface and Coatings Technology, 2017. 318: p. 250-261.
[18] P. Fauchais and A. Vardelle, Solution and suspension plasma spraying of nanostructure coatings, in Advanced Plasma Spray Applications. 2012, InTech.
[19] N.P. Padture, M. Gell, and E.H. Jordan, Thermal Barrier Coatings for Gas-Turbine Engine Applications. Science, 2002. 296(5566): p. 280-284.
[20] I.O. Golosnoy, A. Cipitria, and T.W. Clyne, Heat Transfer Through Plasma-Sprayed Thermal Barrier Coatings in Gas Turbines: A Review of Recent Work. Journal of Thermal Spray Technology, 2009. 18(5): p. 809-821.
[21] E. Litovsky, M. Shapiro, and A. Shavit, Gas pressure and temperature dependences of thermal conductivity of porous ceramic materials: Part 2, refractories and ceramics with porosity exceeding 30%. Journal of the American Ceramic Society, 1996. 79(5): p. 1366-1376.